ELSEVIER

Journal of Structural Geology 29 (2007) 1605–1621

JOURNAL OF STRUCTURAL GEOLOGY

www.elsevier.com/locate/jsg

Vertical and horizontal strain partitioning of the Central Tianshan (NW China): Evidence from structures and $^{40}Ar/^{39}Ar$ geochronology

T.N. Yang [a,*], Y. Wang [b], J.Y. Li [a], G.H. Sun [a]

[a] *Institute of Geology, Chinese Academy of Geological Sciences, Beijing, 10037, China*
[b] *Geological Laboratory Center and Department of Geology, China University of Geosciences, Beijing, 100083, China*

Received 2 March 2007; received in revised form 2 August 2007; accepted 2 August 2007
Available online 14 August 2007

Abstract

As a major tectonic collage within the Central Asia Orogen Belt (CAOB), the Chinese Tianshan provides a natural laboratory for studying structures resulting from the amalgamation of different tectonic units. Detailed field and micro-tectonic observations along two orogen-perpendicular transects identify several structural domains with greatly variable structural styles that were generated at different structural levels but are now juxtaposed. Geological features combined with $^{40}Ar/^{39}Ar$ geochronologic data suggest the variable structural styles of the domains developed simultaneously during ca. 320–300 Ma. Kinematic reconstruction and deformation temperature estimation, taking $^{40}Ar/^{39}Ar$ thermochronological data into account, suggest both horizontal and vertical extrusion of material of the Central Tianshan magmatic arc assemblage (CTMA) crust, which is the expression of heterogeneous strain partitioning during orthogonal continental convergence. Such a kinematic scenario is quite compatible with, and satisfactorily interpreted in the light of the results of available analogue deformation experiments and numerical modeling. The structure styles with orthogonal symmetry of both the CTMA and the southern Tianshan fold-and-thrust belt revealed in this study, in conjunction with previously published paleomagnetic data from the Tarim Plate, suggest that the diachronous collision of the Illi-central Tianshan micro-continent with the Tarim Plate may have caused the Tarim block rotation.

Keywords: Strain partitioning; Fold and thrust; Mylonite; Orthogonal convergence; $^{40}Ar/^{39}Ar$ geochronology

1. Introduction

One major goal of structural geologists is to integrate detailed field observations and kinematic analyses with the larger scale predictions of plate tectonics (Ramsay and Lisle, 2000). Such integration has greatly improved our understanding of the dynamics of convergent margins, a field of study which is still rapidly changing (Ernst, 2005). Perhaps one significant improvement is the recognition that strain partitioning (i.e., flow partitioning at the crustal scale) is a fundamental characteristic of deformation throughout most, if not all, of the Earth's lithosphere during orogenesis (Jones et al., 2005, and references therein). This phenomenon has been viewed as a fundamental consequence of deformation of heterogeneous media, where material heterogeneity is manifest as contrasts in competency (Goodwin and Tikoff, 2002).

The Central Asia Orogenic belt (CAOB) (Hendrix et al., 1992) has attracted considerable attention because of its "juvenile" crustal characteristics that bear information on the Phanerozoic growth of the continents (Jahn et al., 2000a). Numerous petrologic and associated geochemical studies (Jahn et al., 2000b; and references therein) have demonstrated that the CAOB contains the most voluminous block of young continental crust in the world. It is well known that the immense CAOB was formed by both Paleozoic accretion-collision and Cenozoic intracontinental orogenesis, resulting in a mosaic of continental blocks and arc fragments separated by accretionary complexes (Heubeck, 2001), which was

* Corresponding author. Tel.: +86 1 68999722; fax: +86 1 68994781.
E-mail address: yangtn@cags.net.cn (T.N. Yang).

0191-8141/$ - see front matter © 2007 Elsevier Ltd. All rights reserved.
doi:10.1016/j.jsg.2007.08.002

termed the Altaids tectonic collage by Sengor et al. (1993). Thus, the CAOB (or Altaids) provides a natural laboratory for studying the continent growth process including (1) the addition of juvenile crust newly extracted from the mantle, and (2) amalgamation of these juvenile crust units by accretion/collision and subsequent crustal shortening.

A growing body of geological data, particularly that related to petrologic, geochemical, and geochronologic studies (see review of Xiao et al., 2006), has resulted in a new comprehensive tectonic model (Xiao et al., 2004). While the architecture of the CAOB is relatively well established, important questions remain concerning the collage's history of deformation and structural overprinting, the variation in structural styles and associated strain compatibility, and strain partitioning within the orogen. Most previous structural studies focused on deformation along boundaries of tectonic units (Windley et al., 1990; Laurent-Charvet et al., 2003) while few (Xu et al., 2003; Cunningham et al., 2003) have dealt with structures within tectonic units. In other words, intra-unit strain partitioning has typically been overlooked.

In this paper, we document detailed field and microscopic observations along two orogen-normal sections across the Chinese Tianshan collage, focusing on structural features. Kinematic analysis was carried out and used to constrain the horizontal and vertical strain-partitioning scenario. Microscopic observations of minerals in oriented thin-sections reveal deformation mechanisms and constrain temperatures of deformation. The timing of deformation was determined by the $^{40}Ar/^{39}Ar$ method. These observations are interpreted in the light of the results of available analogue deformation experiments (e.g., Rossetti et al., 2002; Cagnard et al., 2005) and numerical modeling (e.g., Upton et al., 2003). Finally, the implications for the collision between the central Tianshan-Illi micro-continent and the Tarim plate are discussed.

2. Geological setting and tectonic units of the Chinese Tianshan collage

The Chinese Tianshan comprises a major tectonic collage within the tremendous Central Asia Orogen Belt (CAOB) (Hendrix et al., 1992). It was formerly thought to have formed during two stages of nearly N–S directed convergence (Windley et al., 1990; Allen et al., 1992): (1) the late Carboniferous collision of the southern Tianshan unit with the central Tianshan unit; and (2) the late Permian collision of the northern Tianshan unit with the central Tianshan unit. It was long ago recognized that the tectonostratigraphy, magmatism, and metamorphism are distinctively different along the length of the Tianshan collage (Hao and Liu, 1993; Chen et al., 1999), implying a complicated diachronous subduction–collision history. Some lines of evidence show that the final collision between the southern Tianshan and the central Tianshan may have extended well into the late Permian (Li et al., 2005; Xiao et al., 2004, 2006) or even Triassic (Zhang et al., 2005). In the western segment of the Tianshan collage, an eastward tapering of a small continent, the Illi-central Tianshan micro-continent (Xiao et al., 1992; Heubeck, 2001) has been identified between the northern Tianshan arc complex and the Tarim craton. Therefore, the western segment of the Chinese Tianshan is commonly divided into three units separated by two suture zones: North, Central, and South Tianshan. Our study area, the Baluntai-Kumish region, is located at the eastern tip of the western segment (Fig. 1).

A confusing array of terminology has been used for the tectonic units of the Chinese Tianshan collage (Xiao et al., 1992; Gao et al., 1998; Chen et al., 1999; Zhou et al., 2001). Here we follow the convention of Zhou et al. (2001) and refer to the three units as the North Tianshan accretionary complex (NTCC), the Central Tianshan magmatic arc assemblage (CTMA), and the South Tianshan fold and thrust belt (STFT). This study focuses on the CTMA and STFT described below.

2.1. Central Tianshan magmatic arc (CTMA)

In the studied eastern segment of the CTMA (Fig. 2), minor Precambrian high-grade metamorphic rocks crop out sporadically, consisting of hornblende-bearing biotite gneiss with amphibolite lenses rich in migmatite veins. Its geologic age has not been positively defined except for a few Sm-Nd model ages of 2500–2300 Ma (Che et al., 1994). Several zircon grains from an early Devonian granitic dyke that intruded in the high-grade metamorphic rocks gave concordant $^{206}Pb/^{238}U$ ages of 2511 ± 34 Ma, 2048 ± 28 Ma, and 1545 ± 16 Ma (SHRIMP analyses, Yang et al., 2006).

Low-grade Proterozoic metasedimentary rocks crop out in the northwest of the study area (Fig. 2). Lithologies include quartzite, fine-grained biotite paragneiss, mica schist, marble, and meta-andesite porphyry with a remnant porphyro-aphanitic texture. Its geologic age is still unclear due to absence of high quality radiometric data. Meso-Proterozoic granite (956 ± 11 Ma, SHRIMP U/Pb dating, Yang et al., in press) intruded in the meta-volcaniclastic rocks, suggesting that the metasedimentary rocks are older than the Meso-Proterozoic.

Cambrian to Ordovician active continental margin volcaniclastic rocks are limited in the northeast portion of the studied area (Fig. 2); similar sequences occur as a belt in the western segment of the CTMA (Xiao et al., 1992). These units consist of low-grade meta-basalt, spilite, keratophre, and greywacke with minor marble and radiolarian chert; together with serpentinized peridotite and gabbro, these units comprise the Gangou ophiolite mélange (Che et al., 1994).

Silurian to early Devonian clastic sedimentary strata unconformably overlie the Gangou ophiolite mélange and other pre-Silurian rocks. Detailed paleontologic, petrologic, and geochemical data demonstrate that the Silurian-Devonian strata formed in an active continental margin (Andean type) environment (Wu et al., 1990). Paleocurrent studies (Wang, 1999) suggests the subducted oceanic crust, which stimulated the Silurian to Devonian CTMA, was located south of the CTMA (the southern Tianshan Ocean, Xiao et al., 1992). This inference was confirmed by new reports of geochemical and radiometric data of magmatic plutons. Numerous calc-alkalic granitic, dioritic, and gabbroic plutons with continent magmatic arc affinities were identified within the studied

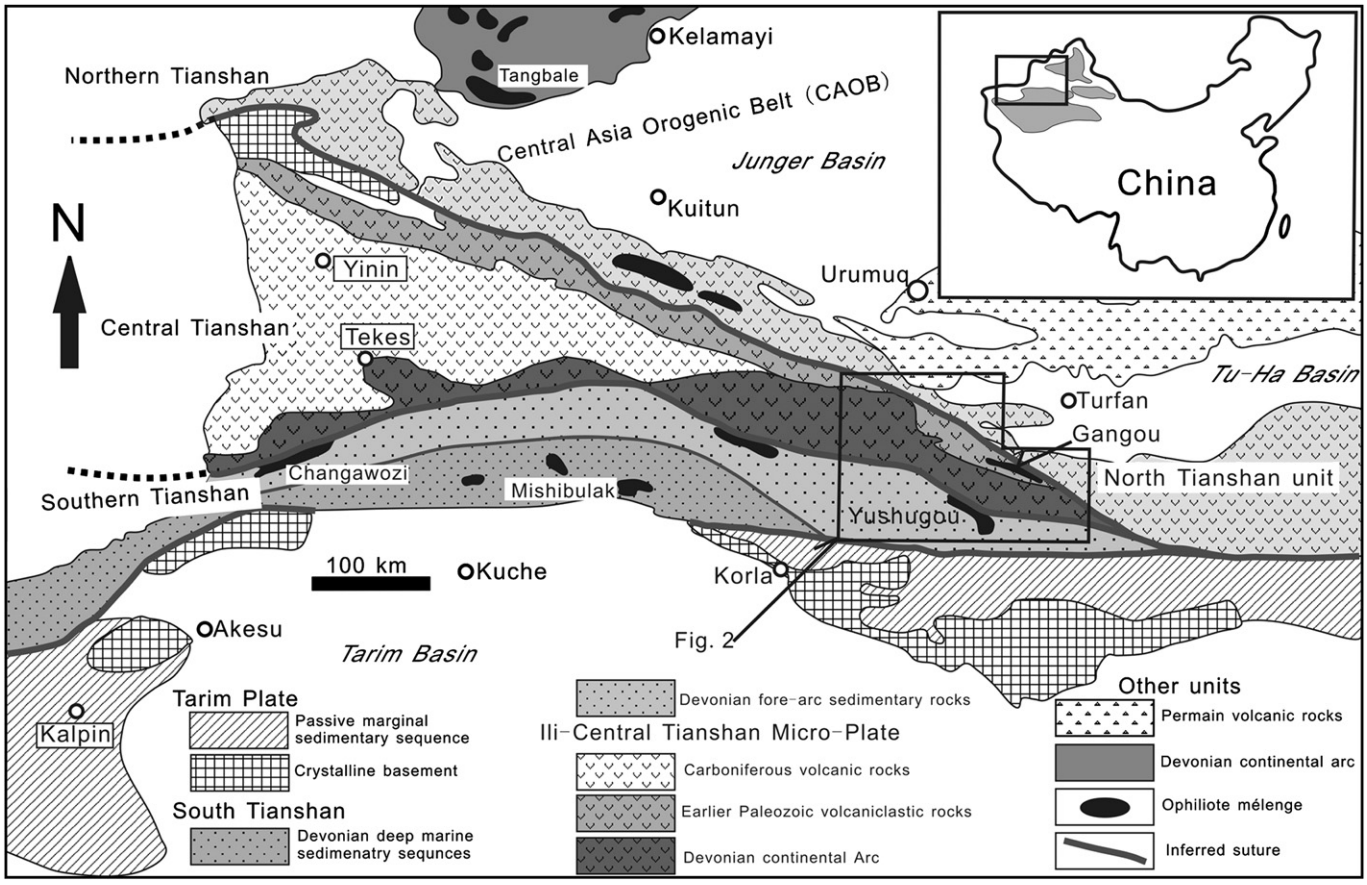

Fig. 1. Regional tectonostratigraphy of the Chinese Tianshan range, NW China. Note that the Illi-central-Tianshan micro-plate has an eastward taper. The study area is labeled.

central Tianshan and yielded SHRIMP U-Pb ages of 392–405 Ma (Yang et al., 2006; Yang and Wang, 2006).

There is a clear gradient in the metamorphic grade that decreases away from the intrusive contact of the early Devonian plutons: near the contact, Grt + Dio + Scp + Ky (mineral abbreviations after Kretz, 1983) assemblages occur together with Bt, Mus, Pl, and Qtz within the country clastic rocks, indicating upper amphibolite-facies metamorphism; far away from the contact, Grt, Scp, Ky, and Dio gradually disappear, forming typical greenschist facies assemblages of Bt + Mus + Kr + Qtz + accessory minerals.

Un-metamorphosed early Carboniferous neritic bioclastic limestone, mudstone, siltstone, and sandstone lie over a basal conglomerate. Locally, these units are found lying unconformably above the Pre-Carboniferous rocks. It is worthy pointing out that volcanic rocks with arc-affinity are uncommon in the studied segment of the central Tianshan although they are widespread in its western counterpart (Zhu et al., 2005), suggesting that subduction of the south Tianshan oceanic crust that shaped the CTMA ceased in the early Carboniferous in the studied area but continued in the western Tianshan.

2.2. South Tianshan fold and thrust belt (STFT)

The Chinese Southern Tianshan was commonly regarded as a passive continental margin of the Tarim Plate, consisting of Early to Middle Paleozoic platform sedimentary rocks (Windley et al., 1990; Allen et al., 1992; Zhou et al., 2001). However, detailed studies (Wang, 1999) demonstrated that the sedimentary rocks in the STFT maybe divided into three tectono-stratigraphic packages (northern, central, and southern), based on their internal characteristics.

The northern package was deposited in a Silurian to Devonian fore-arc basin and mainly consists of volcaniclastic sediment in the lower part and carbonate intercalated with siliciclastic rocks in the upper part. This sequence locally (e.g., Kumish area, Fig. 2) overlaps the CTMA and has thus been thought of as one component of the CTMA.

No pre-Silurian strata have been identified in the central tectono-stratigraphic package. The package is composed mainly of Devonian to Carboniferous dark clastic flysch and calcareous turbidite, indicating a deep marine sedimentary environment, where conglomerate layers are intercalated. From the east (in the studied area) to the west, the grain size of clastic sedimentary material decreases gradually; gypsolith is identified in the upper Devonian strata at the eastern segment suggesting a westward deepening sea basin. Wang (1999) further suggested the eastern part of the south Tianshan oceanic basin closed during late Devonian to early Carboniferous, while its western part evolved to be a west-facing remnant oceanic basin. Several ophiolite fragments crop out locally within this package.

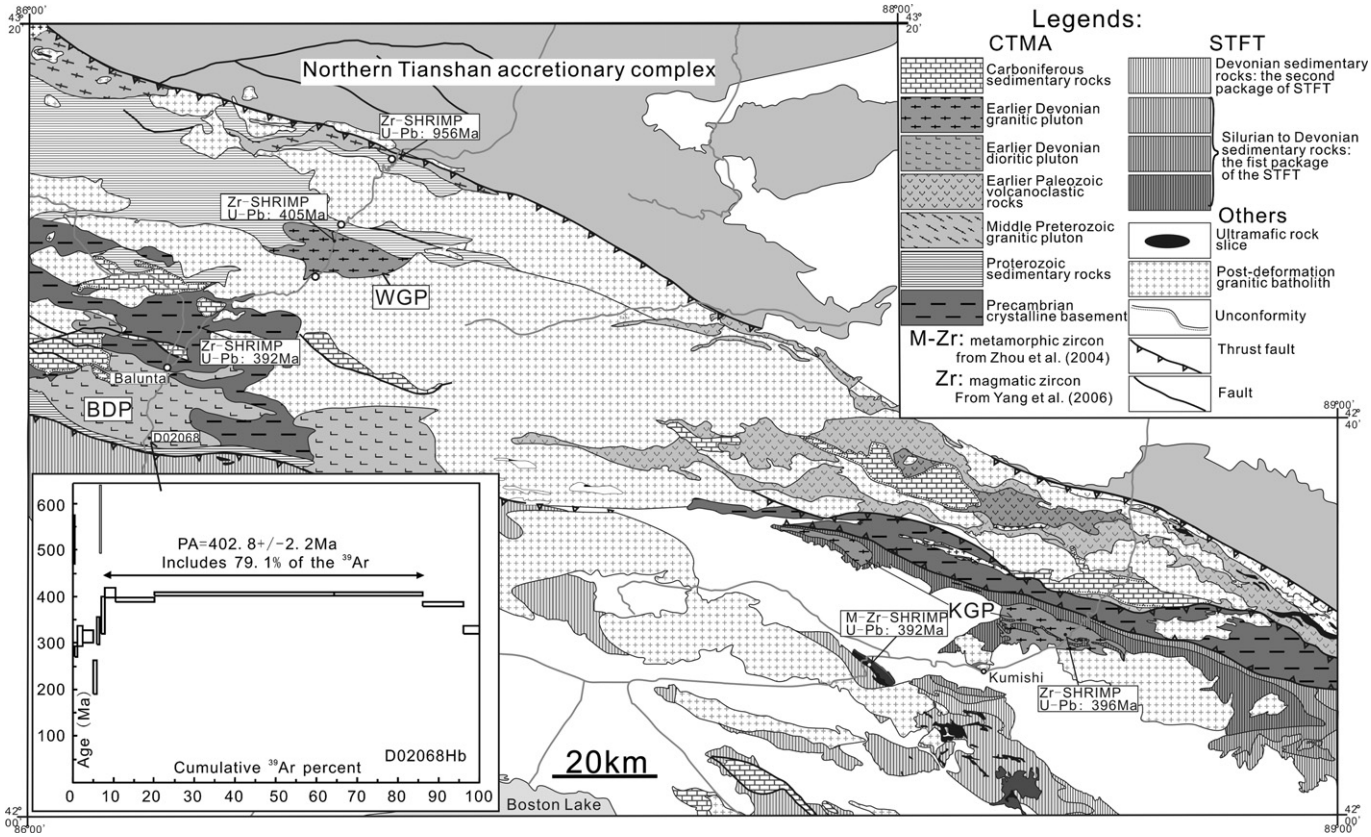

Fig. 2. Geologic map of the Baluntai-Kumish area (modified after six unpublished geological maps, scale 1/200,000. XBGM, 1965, 1971, 1972, and 1975). The inset box shows the $^{40}Ar/^{39}Ar$ age spectra of hornblende from the Baluntai dioritic pluton (sources: Zhou et al., 2004; Yang et al., 2006).

The southern tectono-stratigraphic package consists of Sinian to Permian marine siliciclastic, limestone, and mudstone. There are two major unconformities between (1) the Middle Ordovician and Lower Silurian, and (2) the Devonian to Lower Carboniferous (Carroll et al., 2001), representing the northern passive margin of the Tarim Plate. This package does not crop out in the studied area.

3. Structural observations

Detailed structural observations were carried out along two sections (the Baluntai and Kumish) across the Chinese Tianshan collage. Both of the sections display variable structure patterns and different lithologies. Eight structural domains with different lithologies are defined based on the structure pattern, B-1 to B-4 for the Baluntai section (Fig. 3) and K-1 to K-4 for the Kumish section (Fig. 4).

3.1. Structures of the domains B-1 and K-2

The domains B-1 and K-2 comprise early Devonian granitic plutons intruded, respectively, into (1) Proterozoic metaclastic rocks (Fig. 3; the Wulasitai granitic pluton, WGP), and (2) the core region of a map-scale anticline (Fig. 2; the Kumish granite pluton, KGP) that is manifested by repeated distributions of the Silurian sequences. Deformation features in the two domains include strong mylonitization of the WGP and KGP with the main shear zones having formed along their intrusive contacts; foliation and stretching lineation are defined by elongated quartz and feldspar grains. The structural style of the two domains is slightly different.

3.1.1. Domain B-1

The WGP and its country meta-clastic rocks share common foliation and stretching lineation. The lineation is much clearer than foliation, defining $L \gg S$ tectonites. Stereographic plots of pole to foliation and lineation in the WGP and its country rocks indicate that the foliation is undulating, forming E–W trending, circular, open folds (Fig. 3a, b, and c). Stretching lineations are quite consistent with ESE trends (Fig. 3a).

Local curvature of foliation and S-C fabrics in meta-clastic rocks, as well as other structural criteria including asymmetric folds and porphyroclast systems, mineral fish, and shear bands (Hanmer and Passchier, 1991; Passchier and Trouw, 2005), consistently indicate a top-to-the west sense of shear.

Detail micro-observations revealed that (i) besides layer-parallel shearing and recumbent isoclinal folds, elongation of quartz grains that formed ribbons wrap around slightly elongate feldspar grains, resulting in a mosaic micro-structure (Fig. 5a and inset). It is the same case for weakly deformed granite except for the latter having a coarser grain size (Fig. 5b). This structure is comparable with the interconnected weak layer structure of Handy (1990). (ii) For granitic mylonite, both quartz and feldspar grains are strongly

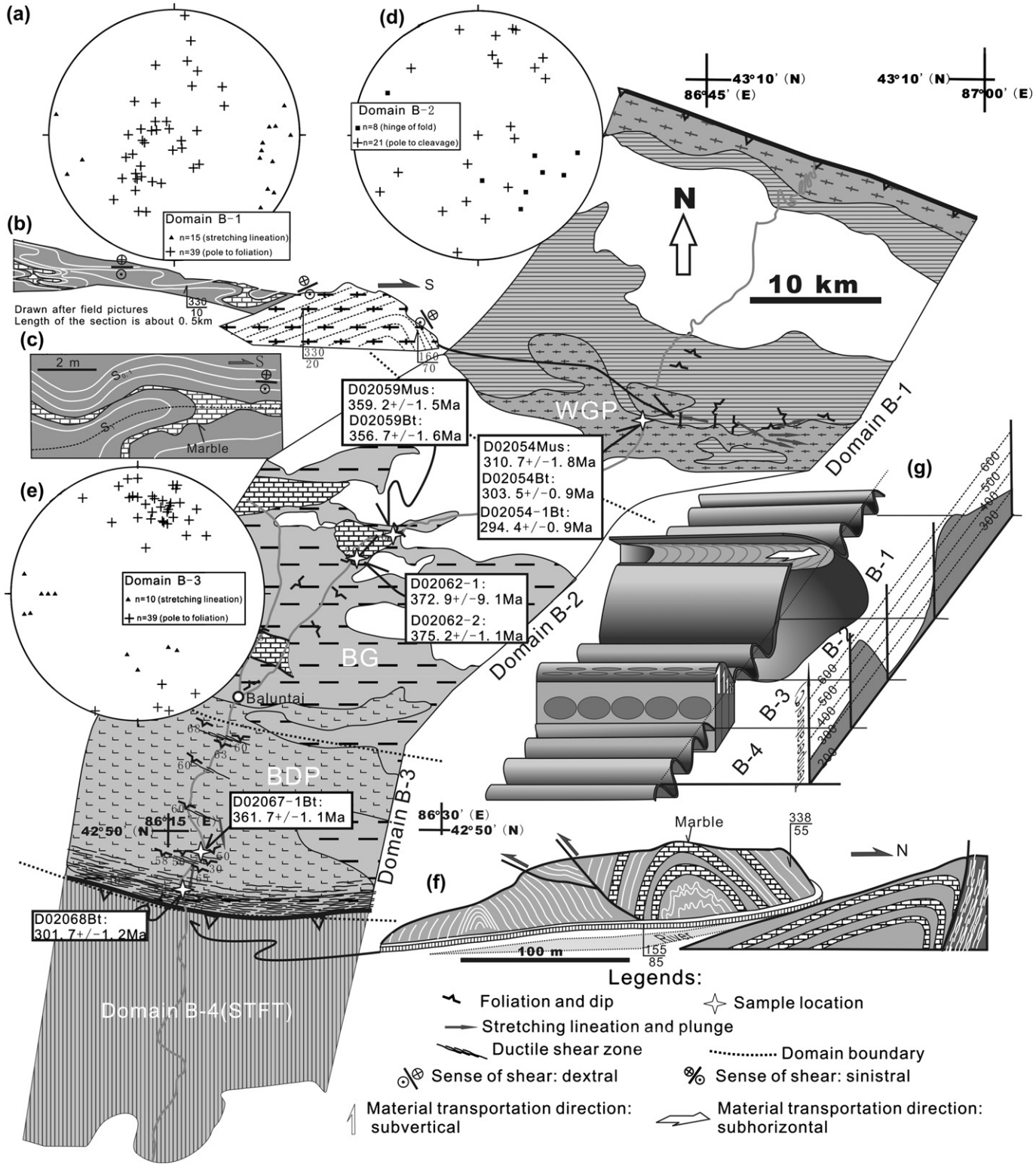

Fig. 3. Structural map of the Baluntai section. The bulk strain for each domain is shown schematically in the 3D sketch diagrams, with a deformation temperature profile (g). Text labels in boxes show location of samples selected for $^{40}Ar/^{39}Ar$ geochronology and their plateau age. The lithologic marks are same as those of Fig. 2. Detailed descriptions are given in the text.

elongated and form ribbons with a very high aspect ratio in the X−Z section such that they look like layers in a thin section scale (Fig. 5c); conversely, the aspect ration in the Y−Z section is very low.

3.1.2. Domain K-2

From the center of the domain to its northern contact of the KGP, the mylonitic foliation displays a curved trajectory (Fig. 4a): in the center, the foliation has N−S strike with

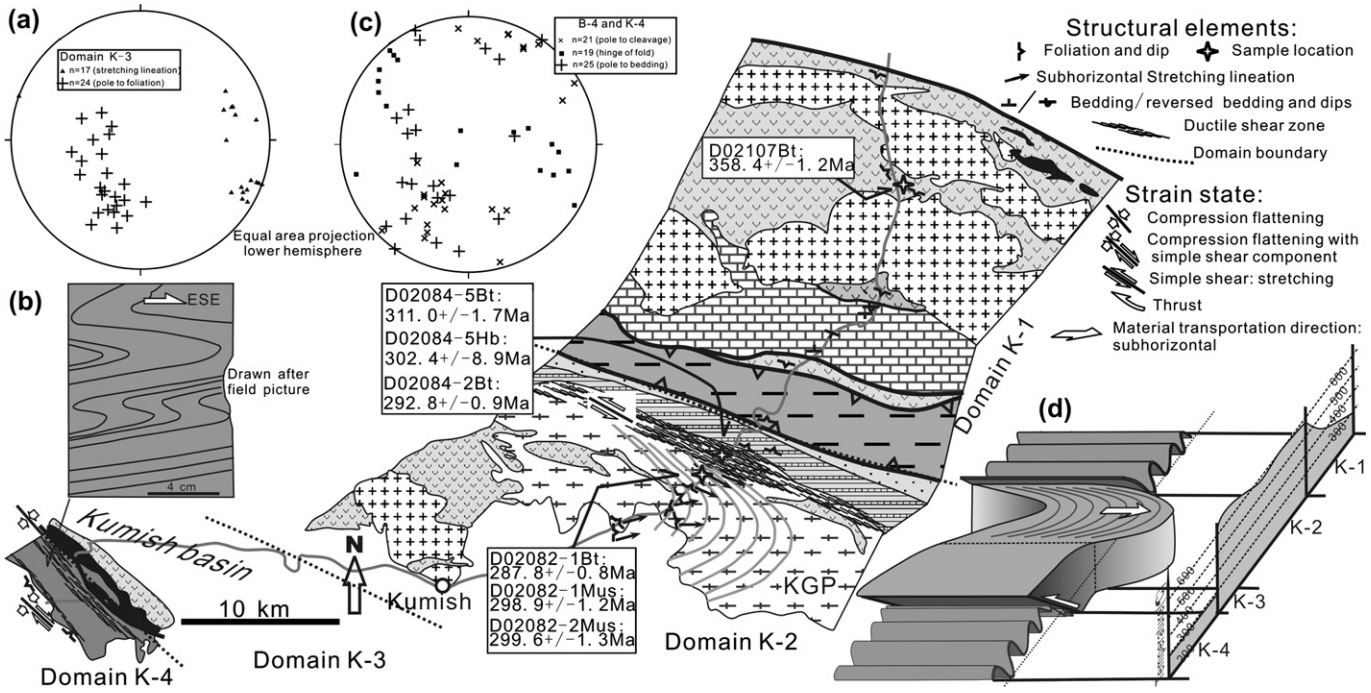

Fig. 4. Structural map of the Kumish section. The bulk strain for each domain is shown schematically in a 3D sketch diagrams, with a deformation temperature profile (d). Other symbols and the lithologic marks (except for the Kumish granite pluton, KGP) are same as those of Figs. 2 and 3. For details, see text.

a moderate dip of 30–45° to the east; northward, the strikes of foliations gradually change to WNW–ESE and the dips increase to nearly 90°. With the change in foliation trajectory, the finite strain of the KGP increases: in the central part, feldspar and Qtz are flattened with the same aspect ratio in the X–Z and Y–Z sections defining S-type tectonite. The tails of the flattened minerals or mineral aggregates are dragged and then progressively merged into a set of parallel planes (C-plane), which is rich in mica, and may be considered as a fabric attractor (Passchier and Trouw, 2005). Upon the C-plane, preferred orientations of elongated mica aggregates and ridge-in-groove slickenside striae (Lin and Williams, 1992) define a lineation with the same dip as the C-plane. In the X–Z section, C-S fabrics are apparent and indicate a top-to-WNW shear sense. In contrast, along the northern intrusive contact, the granite is much more strongly deformed, resulting in augen-mylonite (Fig. 6a). Quartz was stretched into monomineralic ribbon grains with aspect ratios >20 (Fig. 6a and b) in the X–Z section and on the order of 1–2 in the Y–Z section (Fig. 6c); these quartz stretching lineations (L-tectonite) trend WNW–ESE and plunge sub-horizontally. Feldspar was stretched as well, but with a lower X–Z aspect ratio than quartz. In outcrop, the feldspars comprise centimeter-scale porphyroclasts with very long tails. Where the ‘‘isolation factor’’ (Passchier and Trouw, 2005) is high, most porphyroclasts display stair-stepping that indicates a consistent sinistral shear sense (Fig. 6a). If the porphyroclasts are close together, the pattern of stair-stepping defines both antithetic and synthetic extensional crenulations cleavage.

The meta-clastic rocks have a well-defined foliation but lack stretching lineations; even elongate euhedral minerals, such as kyanite (Fig. 7a), are randomly orientated in the plane of the foliation. Field and micro-structural observations reveal that the country rocks have a symmetrical shape fabric both in the X–Z (Fig. 7b) and Y–Z sections. The felsic strain shadows (Fig. 7c) surrounding garnet porphyroblasts has an orthorhombic symmetry as well.

3.2. Structures of domains B-2 and K-1

The domains B-2 and K-1 mainly consist of Precambrian crystalline basement with a few isolated, remnants of Carboniferous sedimentary cover and Ordovician-Silurian low-grade active continental margin volcaniclastic rocks with remnant ophiolite slices (the Gangou ophiolite suit, Che et al., 1994). The deformation of the crystalline basement is not apparent except for the variation in the dip of gneissic foliation (Fig. 3d), which was locally revealed by folding of leucosome veins. Devonian granitic dykes are common in the gneiss and have variable attitude. Vertical, E–W-striking dykes are stretched and form boudins. Those with other attitudes are commonly folded and have a uniform ESE-striking, vertical axial planar cleavage.

The structure of Carboniferous cover strata is characterized by subvertical folds and thrusts (Fig. 8a and b). The folds are open to tight, chevron to circular without any axial planar cleavage. Box folds are not uncommon. Their axial planes are usually vertical, and hinge traces are sub-horizontal with ESE–WNW trends. A décollement zone, which indicates the cover sequence was detached from the basement, was identified locally.

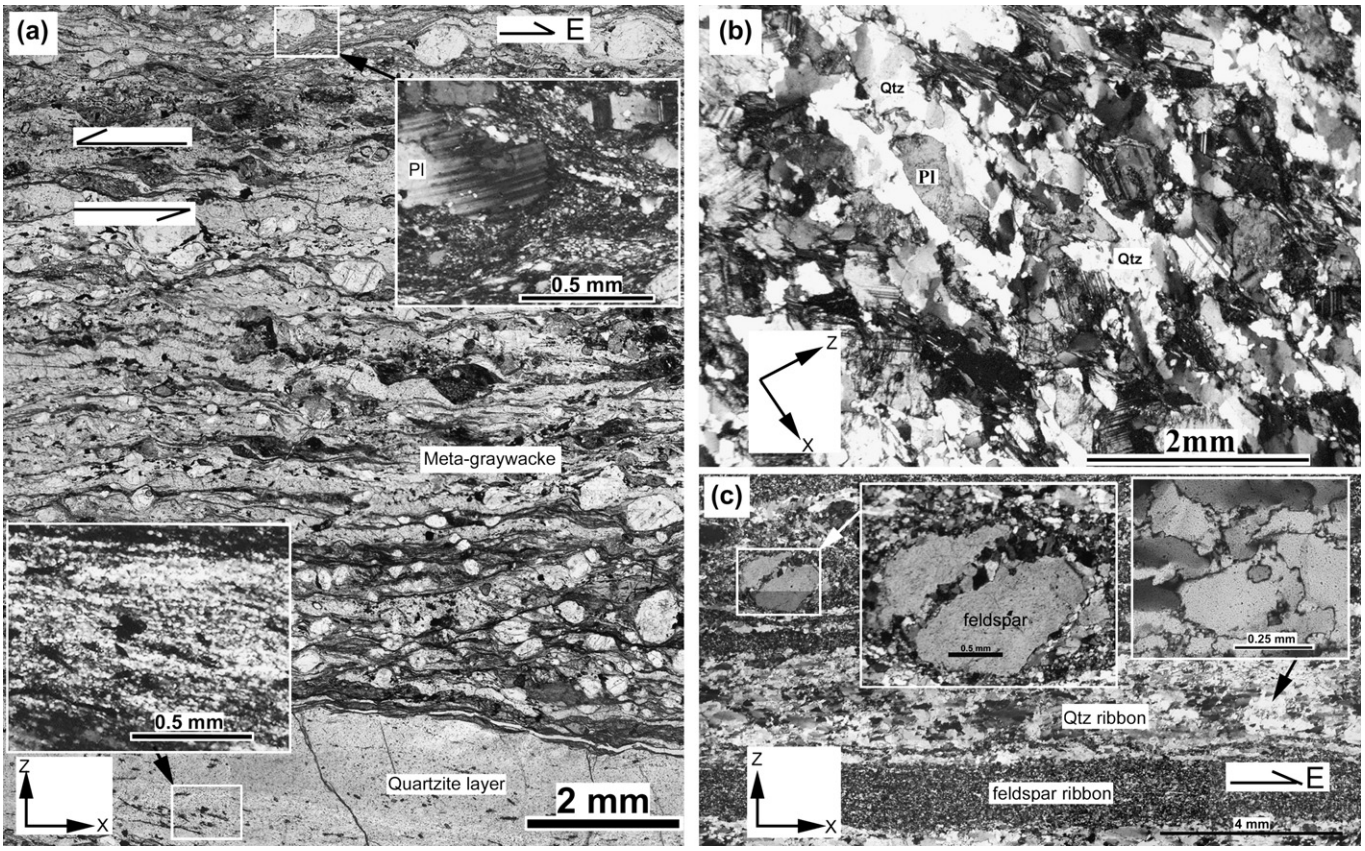

Fig. 5. (a) Micro-photograph (plane polarized light, PPL) shows an overview of a greywacke mylonite from domain B-1. Quartz grains are strongly stretched forming ribbons wrapping around feldspar grains, indicating micro-scale strain partitioning; note that feldspar grains are deformed ductilely as shown by deformation bands and undulating extinction (inset, crossed polarized light, CPL). (b) Micro-photograph of weakly deformed granite with strain accommodated mainly by deformation of quartz, which forms strips surrounding feldspar grain (CPL). (c) Strongly deformed granite. Both quartz and feldspar were stretched into ribbons (CPL). Note feldspar porphyroclast with micro-shear (upper central inset) and very irregular grain boundaries of new quartz grains (upper right inset).

Meter-scale folds are common in the Ordovician to Silurian strata and have tight, circular hinge zones with variable vergence. Although the plunge of the hinge traces is slightly variable, their trajectory is quite stable with an ESE–WNW orientation. No map-scale folds were mapped. Several thrust faults occur along the boundaries between the different lithologic units with different geologic ages, an older unit is commonly thrusted over a younger one. The dips of the thrusts are variable, but most, if not all of them, consistently strike WNW–ESE.

3.3. Structures of domain B-3

The Devonian Baluntai dioritic pluton (BDP) intrudes the Precambrian crystalline basement to the north and meta-clastic rocks (age unknown) to the south in the region comprising the domain B-3. Within this domain, the foliation and strain is not homogeneously developed. Four decameter-scale protomylonite zones within the BDP, and one kilometer-scale mylonite zone (the main shear zone) along its southern intrusive contact are recognized on the basis of the field-data (Fig. 3); they have different structural patterns.

The protomylonite zones in this study refer to bands of incipient mylonitic shear zones within weakly deformed igneous rocks. The foliations are defined by the planar preferred orientation of aligned aggregates of fine-grained biotite and hornblende and flattened plagioclase and quartz. These foliations typically dip between 30 and 70° to the SSW (Fig. 3e). Stretching lineations are not very common and, if present, are defined by ellipsoidal quartz and biotite aggregates that plunge between 30 and 70° to the SSW (down-dip orientation in the foliation plane). Thus, the protomylonite is mainly S-tectonite.

The main shear zone is truncated to the south by a late top-to-the north thrust fault (the Wuwamen fault) considered to be the suture between the CTMA and the STFT (Xiao et al., 1992). Both the BDP and its country metaclastic rocks are strongly mylonitized. Northward away from the intrusive contact, the strain of the BDP gradually decreases as expressed by strain gradient from ultramylonite to undeformed diorite. Most, if not all, small-scale dioritic dykes branching into the country rocks are strongly deformed and form ultramylonite. Foliation and stretching lineation are commonly developed and defined by the preferred orientation of quartz, plagioclase, and biotite; the lineation is generally more developed, defining $L > S$ tectonite. The foliation is generally vertical and strikes WNW–ESE; the plunge of the stretching lineation is shallow (Fig. 3e). At outcrop scale, mineral shape fabrics have an orthorhombic symmetry both in the X–Z and Y–Z sections.

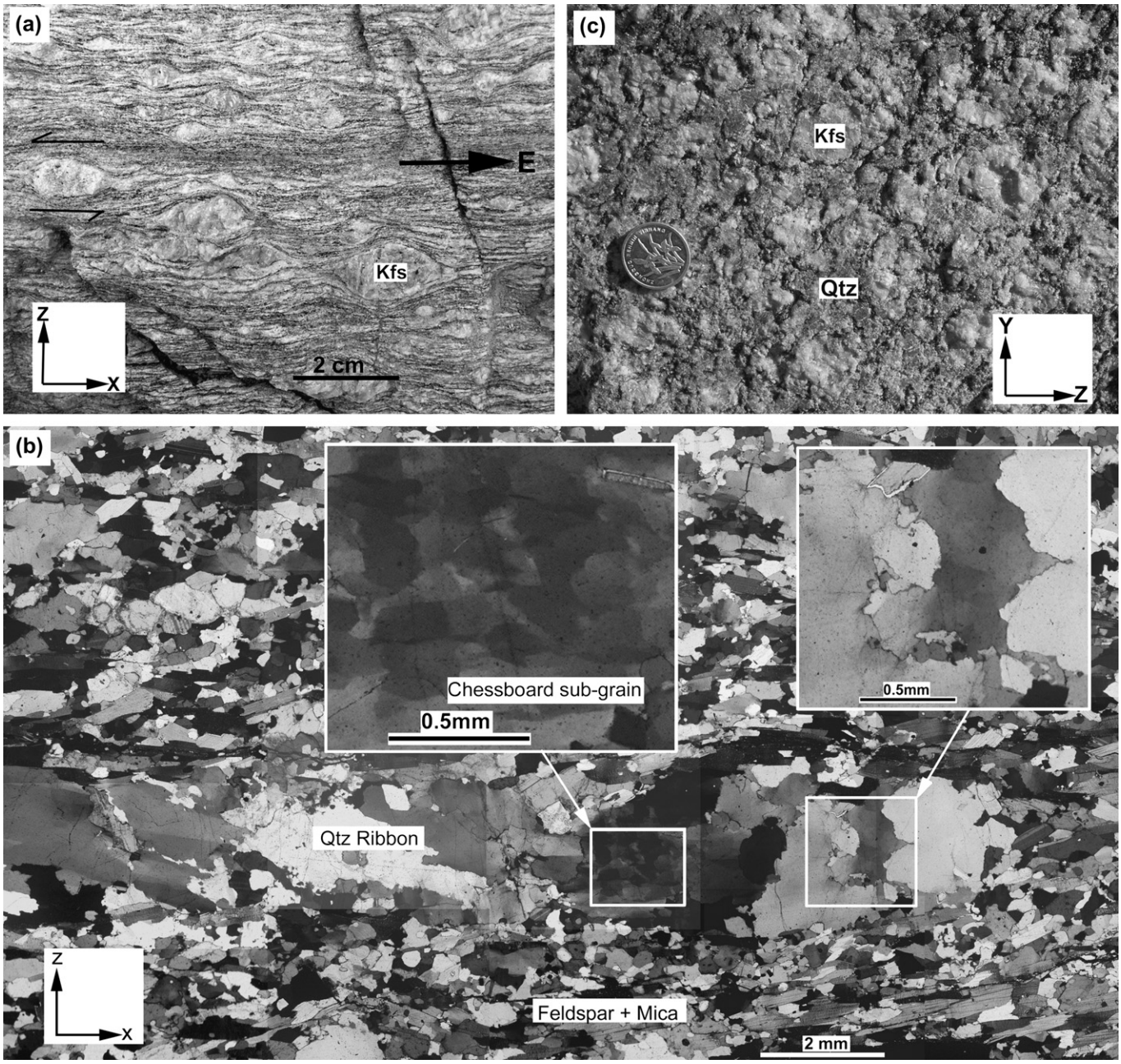

Fig. 6. (a) Augen-mylonite along the northern boundary of the KGP. (b) Micro-photograph (CPL) showing detail of the augen mylonite of (a), chessboard-type subgrains (central inset) and irregular boundaries of new grains (right inset) of deformed quartz suggest high-temperature deformation. (c) Along the Y–Z section, the granitic mylonite exhibits equi-granular grain (or aggregates) shape. (a) and (c) represent an L-tectonite from the same outcrop.

In the protomylonitic rocks, plagioclase and hornblende have a grain size of 1–5 mm and constitute a load-bearing framework, while quartz has an irregular morphology and occupies interstitial spaces. Deformation of hornblende is characterized by intragranular fractures, the orientations of which are mainly controlled by cleavages.

With increasing strain, 20–80 μm plagioclase grains form at the margin of, or along micro-shear zones within old plagioclase grain, dividing the old grain into several domains. The remnants of old grains are surrounded by a moat of recrystallized fine grains, resulting in core and mantle structure (Fig. 9a). The boundaries between the core and mantle are irregular and lobate with lobes on the scale of the new grains indicating that the recrystallization mechanism for the plagioclase is bulging recrystallization. Marginal parts of some hornblende grains were milled into fine angular fragments, some of which are replaced by neocrystalline biotite. Grain boundary migration is the dominant recrystallization mechanism for quartz and is manifested by the variable size of the new quartz grains with irregular grain boundary geometries, and the cuspate-lobate morphology of the ribbon-shaped quartz aggregates (Fig. 9b).

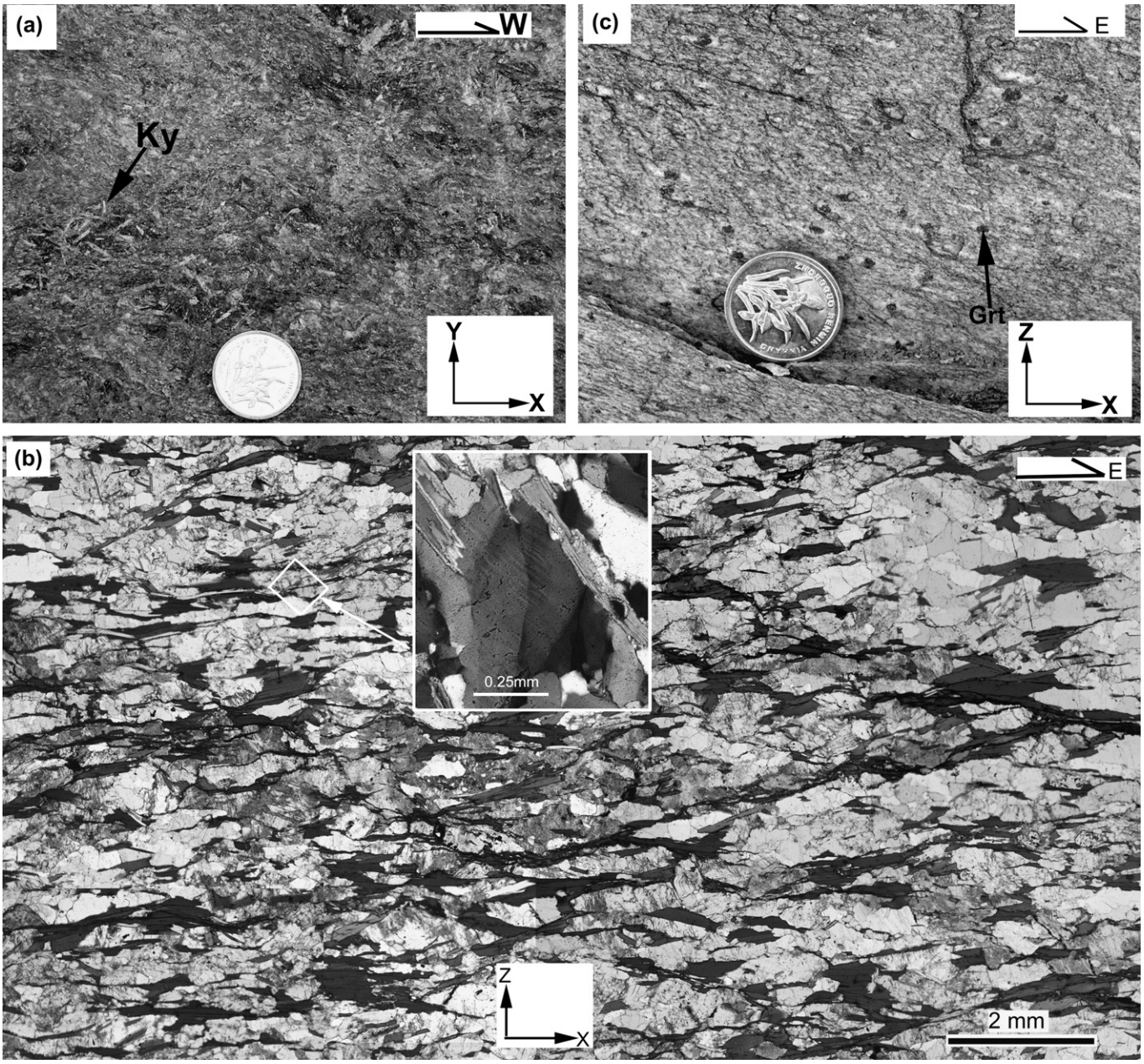

Fig. 7. (a) Elongated kyanite randomly distributed on foliation; (b) the country rocks of the KGP have symmetrical grain-shape-fabric in X–Z sections which is shown by preferred orientation of biotite flakes (PPL). Quartz is deformed ductilely (inset, CPL). (c) Felsic strain shadows of garnet porphyroblasts have a symmetrical shape as well.

The dragged tails of fine new grain aggregates merge into micro-shear zones (surrounding centimeter-scale large porphyroclasts), defining C′-type-like shear band cleavage. In an X–Z section, two sets of C′-type-like shear band cleavage occur with the same degree of obliquity to the mylonitic foliation at an angle of 30–35°. The two sets of C′-type-like shear band cleavage with reversed shear sense directions and opposite vergence display an orthorhombic symmetry. The two sets of shear band cleavage conjugate at an angle of ca. 110°, consistent with the prediction of the maximum effective moment criterion of Zheng et al. (2004).

In the mylonitic rocks, plagioclase and quartz ribbons form monomineralic layers and wrap around lensoid plagioclase and hornblende porphyroclasts, forming typical core-and-mantle structure (Fig. 9c). Some fine hornblende grains form along old hornblende grain boundaries; locally they develop into fine grain ribbons where very fine neocrystalline biotite is common. Meanwhile, the conjugate angle between the two sets C′-type-like shear band cleavages decreases and asymmetric intrafolial folds (Davis and Reynolds, 1996) are common in the layered mylonite but lack a consistent vergence (Fig. 9c). No new foliation was identified, suggesting the intrafolial

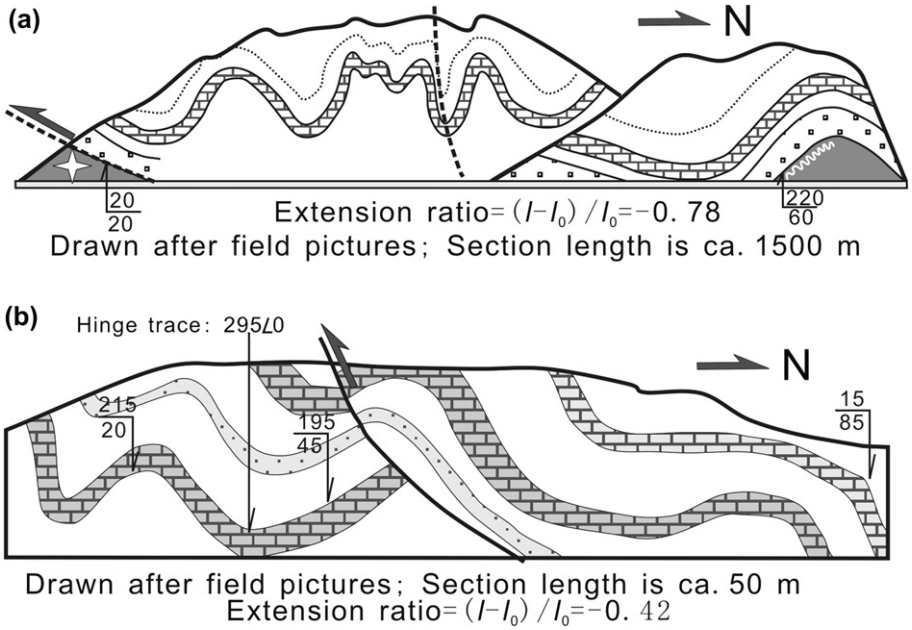

Fig. 8. Structural profiles (drawn after field pictures) show structures in the Carboniferous strata. Note that the extension ratio in domain B-2 (a) is larger than that of domain K-1 (b).

fold resulted from progressive strain. In ultra-mylonite, grain size of nearly all minerals is intensively reduced, and fine grains of different minerals are completely mixed resulting in a homogeneous fine grain matrix where plagioclase porphyroclasts are locally embedded (Fig. 9d). The C′-type shear band cleavage completely disappears in the fine grained matrix of ultra-mylonite, but is preserved in plagioclase porphyroclasts (Fig. 9d).

The micro-structures in the Y–Z sections are generally similar with those in the X–Z sections. The structures in both the X–Z and Y–Z sections have orthorhombic symmetrically shaped fabrics.

3.4. Structures of domains K-3, K-4, and B-4

Domain K-3 comprises an ophiolite suit (the Yushugou ophiolite) consisting of metamorphic peridotite, ultramafic-mafic cumulate, and tholeiite. Petrologic studies (Wang et al., 1998) demonstrated the ophiolite was affected by a granulite-facies metamorphic overprint. A normal brittle fault forms the boundary between the suite to the north and the Kumish Mesozoic basin, while its southern boundary is a thrust with a moderate dip of 40–60° to the NNE. The granulite-facies ophiolite suit is thrust southward over a low-grade sedimentary sequence (domain K-4). Although a few ductile deformation features were identified within the ophiolite suit, it is generally intact. The strain is mainly accommodated along the southern boundary thrust. The large gap in metamorphic grade between the ophiolite suit and domain K-4 suggests the displacement along the thrust is significant.

Domain K-4 comprises a very low grade metasedimentary sequence (the central package of the STFT) consisting of conglomerates at the base, layered sandstone in the middle, and shale intercalated with minor thin limestone in the upper segments. Comprising the footwall of the thrust, the upper segment of the sequence (soft mudstone and limestone) is strongly deformed resulting in a penetratively spaced cleavage (Fig. 10a), which completely transposes the primary bedding. The cleavages are in fact a set of parallelly orientated minor shear zones striking WNW–ESE with dips of 30–50° to the NNE. Thin limestone layers are strongly stretched forming elongated lensoids that define a down-dip stretching lineation. Lensoids commonly have two tails along its tips with monoclinic shape symmetry. The tips of the tails lie at different elevation on both sides, resembling a σ-type object (Passchier and Trouw, 2005) or Group 2 mineral fish (ten Grotenhuis et al., 2003). Synthetic extensional crenulation cleavage or C′-type shear band cleavage is commonly developed and indicates a top-to-the SE shear sense.

About 500 m away from the domain boundary, the cleavage starts to disappear and, as a result, primary sedimentary structures are present. Limestone layers intercalating within mudstone are stretched giving rise to connected boudins with a symmetrical morphology (Fig. 10b). The boudins have similar aspect ratios in both the X–Z and Y–Z sections, suggesting a coaxial flatting strain normal to strata bedding. Southward, the structures of layered sandstone, mudstone, and limestone are featured by large amount of mesoscale folds (Fig. 4b). Most, if not all, folds belong to the Class 2 fold of Ramsay (1967) marked by nearly identical curvatures of their inner and outer arcs. The axial plane of the folds have a uniform strike of WNW–ESE with a moderate to steep dip of 50–70° to the NNE. However, the plunges of their hinge traces are randomly distributed within the uniform axial plane (Fig. 4c). Axial planar cleavage has not developed.

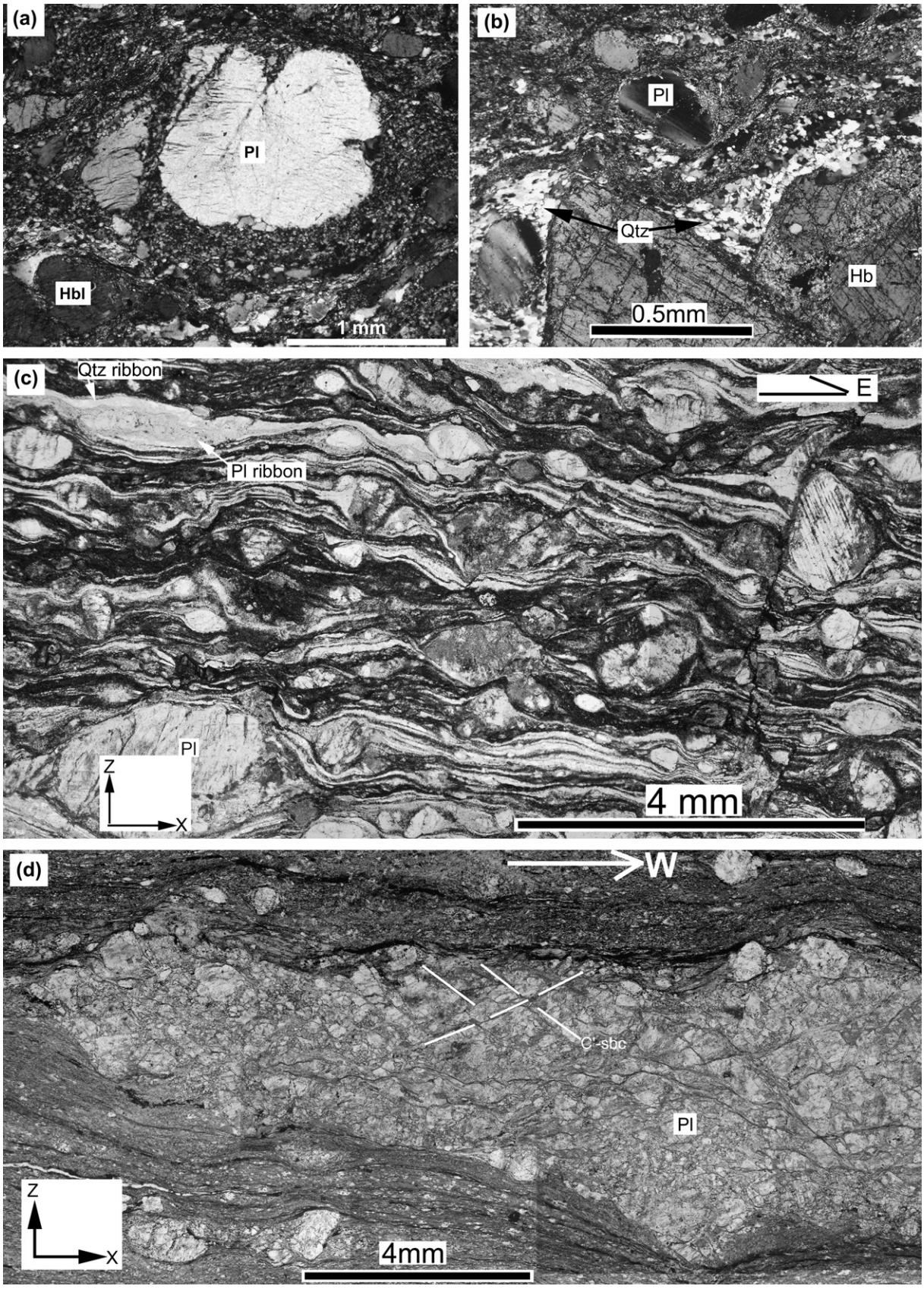

Fig. 9. Micro-photographs from the domain K-3. (a) Core-and-mantle structure in dioritic protomylonite (CPL); (b) new quartz grains with highly irregular boundaries developed in dioritic protomylonite (CPL). (c) Mineral ribbons developed in dioritic mylonite containing a few intrafolial folds (PPL). (d) A large plagioclase porphyroclast embedded in a fine matrix of dioritic ultramylonite (PPL), note the two C′-type shear band cleavages conjugate at an angle of ca. 110°.

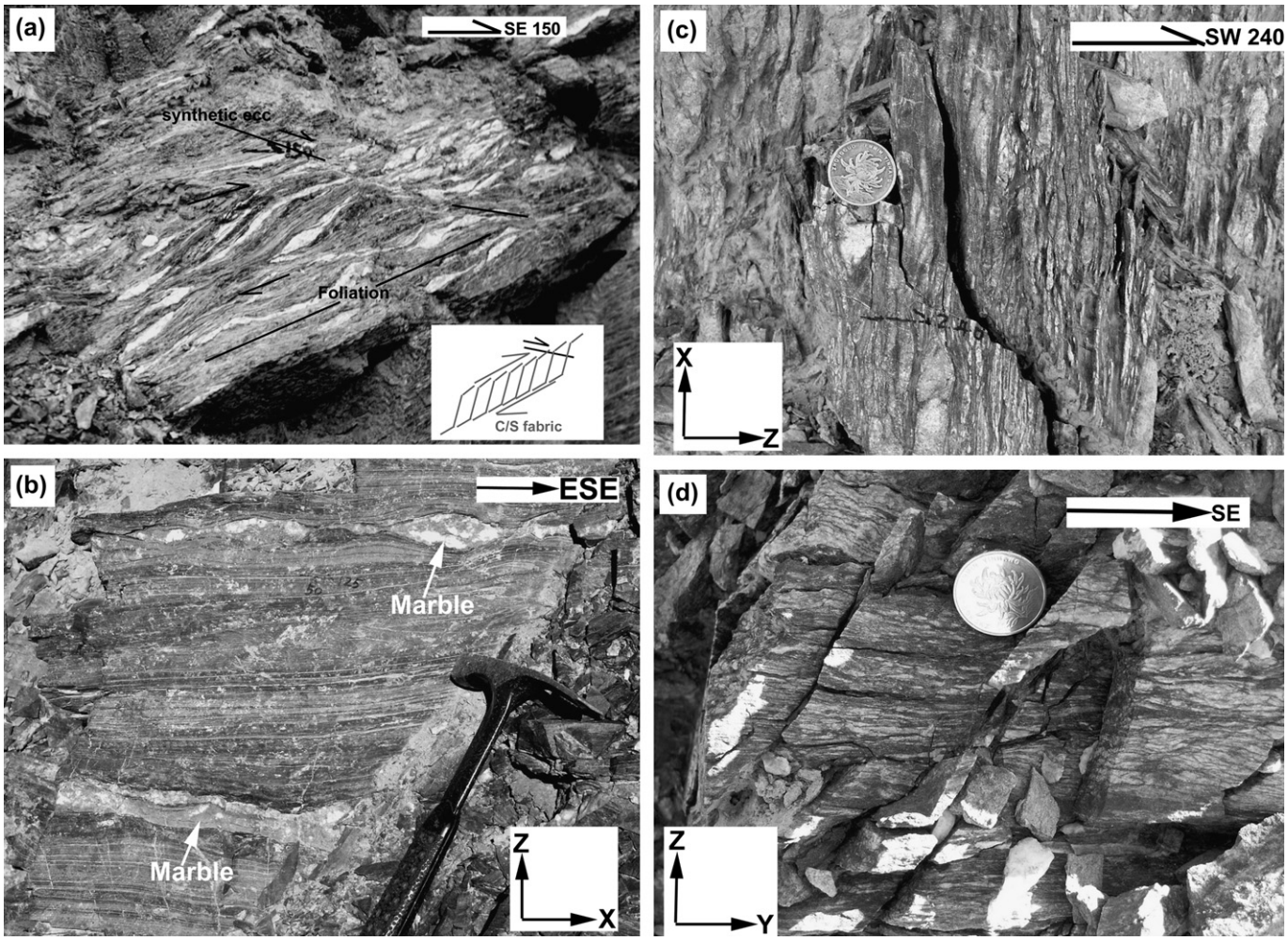

Fig. 10. (a) Pervasive shear zones in the ductile thrust zone between the domains K-3 and 4. S-C fabric and synthetic extensional crenulation cleavage indicate a top-to-the-south shear sense. (b) Symmetrical boudinage of marble layers surrounded by softer mudstone. (c) and (d) pebbles in conglomerate were strongly flattened giving rise to a vertical foliation. Their aspect ratios in X–Z (c) and Y–Z (d) sections are nearly identical corresponding to an S-tectonite.

The southern segment of domain K-4 consists mainly of massive conglomerate without obvious layered structure. No folds were identified. However, pebbles of the conglomerate are strongly flattened defining a vertical foliation. Field observations demonstrate that the aspect ratios (up to 20) of the flattened pebbles in vertical and horizontal sections normal to the foliation are identical (Fig. 10c and d), defining S-tectonite. The foliation is sub-vertical and strikes WNW–ESE. No lineation was identified on the foliation.

The structural pattern of domain B-4 is manifested by numerous hundred-meter scale anticlines and synclines separated by mid- to high-angle thrust faults (i.e., fold-and-thrust structure). Detailed field observations reveal that the folds are generally tight with rounded hinge areas. Their axial planes consistently strike ESE and dip variably to the NNE or SSW, indicating double vergence. Fan-like axial planar cleavage is commonly developed. The thrust faults also strike ESE, and dip NNE or SSW, just like the axial planes of folds. Fig. 3f shows a typical structural pattern of the fold and thrust assemblage. Locally, two thrusts with opposite vergence delimitate a triangular block that is pushed up, forming the pop-up structure.

4. $^{40}Ar/^{39}Ar$ geochronology

4.1. Sampling and analytical methodology

In order to constrain the timing of deformation, 12 samples were taken from different structural sites for mica and/or hornblende mineral separates for $^{40}Ar/^{39}Ar$ step-heating geochronological analyses. The sample locations are shown in Figs. 3 and 4; their mineral assemblages, plateau ages or preferred ages, isochron ages (with MSWD), and J-factors are listed in Table 1. The age dating was completed on a Micromass 5400 mass spectrometer in the China University of Geosciences (Beijing). The J factor was estimated by replicate analysis of Fish Canyon Tuff sanidine with an age of 27.55 ± 0.08 Ma (Lanphere and Baadsgaard, 1997) with 1% relative standard deviation (1σ). The age spectra and classic isotope correlation plots are established using the ISOPLOT program v3.0 (Ludwig, 2003). The error of plateau age is given as 1σ. Weighted mean plateau ages (WMPA) are reported where >50% of the ^{39}Ar released in contiguous steps is within 1σ error. For disturbed spectra, preferred ages (PA) are reported

Table 1
Summary of the $^{40}Ar/^{39}Ar$ geochronological data and petrologic features of the analyzed samples

Sample	Rock	Mineral assemblage	T-Miner.	Loc	*J*-value	PA (Ma)	IA (Ma)	MSWD
D02054-1	G-My	Kfs + Pl + Qtz + Bt + Ms + M-Hbl	Bt	B-1	0.002142	294.4 ± 0.9	296.5 ± 3.1	2.8
D02054	G-My	Kfs + Pl + Qtz + Bt + Ms + M-Hbl	Ms	B-1	0.0024715	310.7 ± 1.8	317.4 ± 4.8	5.0
			Bt		0.002335	303.5 ± 0.9	307.2 ± 5.3	1.4
D02059	Gneiss	Qtz + Pl + Kfs + Bt + Ms + Hbl	Bt	B-2	0.0024745	356.7 ± 1.6	375.0 ± 4.7	106
			Mus		0.0024675	359.2 ± 1.5	365.5 ± 2.8	1.6
D02062-1	Gneiss	Qtz + Pl + Kfs + Bt + Ms + Hbl	Bt	B-2	0.002341	?	372.9 ± 9.1	3.4
D02062-2	Gneiss		Mus	B-2	0.002344	375.2 ± 1.1	377.7 ± 6.3	0.25
D02067-1	D-P-My	Pl + Hbl + Bt + M-Qtz	Bt	B-3	0.002460	361.7 ± 1.1	368.2 ± 2.9	2.7
D02068	D-My	Pl + Hbl + Bt + M-Qtz	Bt	B-3	0.002129	301.7 ± 1.2	318.0 ± 7.1	5.6
			Hbl		0.00209	402.8 ± 2.2	406 ± 13	1.8
D02082-1	G-My	Kfs + Pl + Qtz + Bt + Ms + M-Hbl	Bt	K-2	0.002116	287.8 ± 0.8	289.1 ± 0.5	5.6
			Mus		0.0024729	298.9 ± 1.2	299.1 ± 2.6	0.82
D02082-2	G-My		Mus	K-2	0.002476	299.6 ± 1.3	300 ± 11	6.9
D02084-2	G-My		Bt	K-2	0.002103	292.8 ± 0.9	294.9 ± 1.4	5.8
D02084-5	G-My		Bt	K-2	0.0024645	311.0 ± 1.7	312 ± 3.0	32
			Hbl		0.002347	?	305 ± 35	2.8
D02107	Gneiss	Qtz + Pl + Bt + Mus	Bt	K-1	0.0024615	358.4 ± 1.2	358 ± 7.0	64

G, granitic; My, mylonite; D, dioritic; P, proto-; M, minor; Loc, structural location; PA, plateau age; T-Miner., target mineral; IA, isochron age.

where the spectrum is relatively flat but does not meet the strict criterion for a WMPA. For relatively rapid cooling rates, the estimated closure temperatures are selected as 500 ± 50 °C (hornblende), 400 ± 50 °C (muscovite) and 335 ± 50 °C (biotite) (Harrison et al., 1985; Hames and Bowring, 1994; McDougall and Harrison, 1999). All data are given in supplementary Table 1; Supplementary Fig. 1a, b, and c show the age spectra and classic isotope correlation plots.

4.2. Analytical results

Seventeen separates including nine biotite, six muscovite, and two hornblende, were analyzed using $^{40}Ar/^{39}Ar$ method. Of the 15 analyses that yielded acceptable WMPA and isochron age (IA), ten have identical WMPA and IA within the analytical error; for the other five analyses, the values of the isochron ages are commonly older than those of the WMPA. The seventeen analyses appear to be clustered into three groups.

Group 1 contains only one analysis, that of D02048 hornblende. Its WMPA is 402.8 ± 2.2 Ma (79.1% of the ^{39}Ar released) and is concordant with the isochron age (IA) of 406 ± 13 Ma (MSWD = 1.8) that includes all steps (Fig. 2, inset).

Group 2 includes six analyses from weakly deformed domains. The samples yielded plateau ages and IAs that range from 357 to 375 Ma and from 358 to 375 Ma, respectively.

Group 3 consists of ten analyses, all of which come from strongly deformed mylonite. Their plateau ages range from 287 to 311 Ma with IAs that range from 294 to 318 Ma, similar to each other within error.

It is worthwhile pointing out that the plateau ages of the muscovite are commonly 7–10 Ma older than those of the biotite if they were taken from the same locations within a mylonite zone (compare D02054 Bt and Mus; D02082-1 Bt and Mus; D02082-2Mus and D02084-2Bt, Table 1), but the disparity is much lower (<2 Ma) for those sampled from the same location within a weakly deformed domain (compare D02059 Bt and Mus).

4.3. Interpretations

Sample D02048 (group 1) is a weakly foliated quartz diorite consisting of Pl + Hbl + Bt + minor Qtz. Micro-structural observations demonstrated that the analyzed hornblende in the sample does not display any evidence of plastic intracrystalline deformation, whereas, the biotite was partially crushed and kinked. The age of the sample D02048 Hbl 402.8 ± 2.2 Ma, overlapping with published zircon U-Pb SHRIMP ages (392–405 Ma, Yang et al., 2006; Yang and Wang, 2006) of the calc-alkalic intrusions in the CTMA. It is reasonable to consider the BDP as one member of the central Tianshan calc-alkalic intrusive suit, and the age of ~403 Ma may represent the solidification or cooling age of the BDP.

Samples from Group 2 were collected from the crystalline basement (micaceous gneiss) and weakly deformed, fine grained paragneiss. The six analyses give WMPAs ranging from 357 to 375 Ma, similar to, or older than, the Lower Carboniferous (359 Ma) sedimentary sequence. The geologic meaning of this is not obvious. Field observations demonstrated that the analyzed micaceous gneiss was strongly affected by a thermal event associated with the earlier Devonian magmatic intrusion (392–405 Ma, zircon U-Pb SHRIMP ages; Yang et al., 2006; Yang and Wang, 2006). Some of the micas grew or recrystallized as a result of contact metamorphism. The early Carboniferous non-metamorphic sedimentary sequence overlies the gneiss and both were deformed at ca. 320 Ma. We suggest that the mica $^{40}Ar/^{39}Ar$ ages ranging from 375 to 357 Ma indicate a heterogeneous cooling rate for different part of the central Tianshan magmatic arc before the Carboniferous. The late Carboniferous deformation did not reset the K-Ar isotopic system of the mica completely.

The Group 3 mineral separates are from strongly deformed mylonite zones, where primary magmatic biotite grains were strongly deformed resulting in small fragments that are clustered in strips. Meanwhile, muscovite formed during the

deformation in some mylonite and then deformed during progressive deformation. Micro-structural observations presented in this paper demonstrate that the mylonite developed under high temperature conditions, thus the K-Ar isotope system of the primary magmatic biotite was likely completely reset during the deformation. Because the closure temperature of muscovite is commonly thought to be higher than biotite, the muscovite $^{40}Ar/^{39}Ar$ ages provide a minimum deformation age ($\geq$318 Ma). At ca. 285 Ma, all of the mylonites were exhumed to a crustal level where the temperature was lower than the closure temperature for argon in biotite (ca. 335 $\pm$ 50 °C).

A similar tectonothermal history of the CTMA was recently proposed by Li et al. (in press). They reported detailed monazite Th/Pb-U/Pb centroid ages through the electron microprobe method from the Baluntai-Kumish area, revealing two distinct age groups with probability density peaks at ca. 360 Ma and 320 Ma respectively for the CTMA. These data (although with a larger error due to the shortcomings of the method) are roughly in agreement with our $^{40}Ar/^{39}Ar$ results reported in this paper.

In summary, detailed $^{40}Ar/^{39}Ar$ analyses indicate that all main ductile shear zones with high finite strain within the Chinese Central Tianshan are nearly coeval, developed during ca. 320–300 Ma. This conclusion and the detailed structural data presented in previous sections provide a strong foundation to discuss the kinematic scenario of the CTMA, which may have resulted from the continental collision between the CTMA and the Tarim Plate.

5. Discussion

5.1. Estimation of deformation temperatures

It is notoriously difficult to estimate metamorphic P–T conditions for meta-granitoids due to the consistency of mineral assemblages across a variety of P–T conditions; this stands in contrast with meta-pelitic or meta-mafic rock systems (Spear, 1993). Below we estimate the P–T conditions attending deformation on the basis of the correlation between metamorphic grade during deformation and geometry of particular structures (Passchier and Trouw, 2005), taking into account the $^{40}Ar/^{39}Ar$ data in this study.

The structures of domains B-2, K-1, and K-4 are mainly featured by chevron to circular folds without axial-planar cleavage and a few brittle faults. No new minerals, not even chlorite and sericite, grew during deformation. The strain is pervasive and distributed, and the decoupling is weak between the crystalline basement and its cover. These observations suggest the folds formed under very low temperature conditions (maybe lower than 200 °C). This value is consistent with the fact that the deformation has not reset the K-Ar isotopic system of biotite and muscovite (samples D02062-1, 2, and D02059; see Fig. 3).

Domain B-4 displays fold-and-thrust structural patterns with a well developed axial planar cleavage where sericite and chlorite, and locally, muscovite exhibit preferred orientations, suggesting sub-greenschist facies metamorphic conditions during deformation at temperatures of 200–300 °C.

In contrast, deformation in the other domains is characterized by numerous ductile shear zones. Within the shear zones, minerals have deformed by ductile flow via a range of deformations mechanisms. Studies on experimental and naturally deformed rocks have led to a well established interrelationship between deformation mechanisms and physical conditions; of these conditions, temperature is the most significant (temperature gauge; Passchier and Trouw, 2005). According to the criteria for dynamic recrystallization recommended by Passchier and Trouw (2005), detailed micro-tectonic observations have given rise to the following conclusions: (1) feldspar in granitic mylonite and plagioclase in dioritic mylonite recrystallized through bulging recrystallization (Figs. 5c and 9a). No evidence of subgrain rotation was identified for recrystallization of the feldspar or plagioclase. (2) Quartz in the shear zones recrystallized through high temperature grain boundary migration (Figs. 5, 6b, and 9b).

These observations suggest that the deformation temperature of the ductile shear zones is higher than ~500 °C (lower temperature threshold for grain boundary migration in quartz), but lower than ~600 °C (minimum temperature threshold for sub grain rotation in feldspar). The K-Ar isotopic system likely experienced open behavior to argon diffusion during the deformation; our $^{40}Ar/^{39}Ar$ analyses (see above discussion) suggest this crustal segment passed through the 335 $\pm$ 50 °C isotherm in late Carboniferous (ca. 300 Ma).

The above estimation is shown schematically in Figs. 3g and 4d, demonstrating significantly variable distribution of temperatures of deformation along the two transects. It is obvious that all high-temperature deformation occurred in magmatic intrusions or their adjacent country rocks. There may be two possible causes for such a temperature distribution: (1) local variation in heat flow (high geothermal gradient) resulting from magmatic activation; or (2) divergent vertical extrusion of middle crustal slices causing juxtaposition of middle and upper crustal slices. We prefer the second one, because: (i) the size of domains with different thermal regimes is small (on the scale of 10 km) and at several domain boundaries the gap in temperature is large (up to 300 °C). (ii) Geochronological data indicate that deformation occurred at ca. 100 Ma later after the magmatic intrusions. (iii) The sporadically distributed earlier Carboniferous cover might have been deposited in a stable shallow marine basin based on correlative sequences, implying that entire CTMA may have been covered by the sedimentary sequence. Sporadic remnants of the basin sedimentary rocks reflect heterogeneous uplifting of the CTMA. Thus, we suggest that the distribution pattern of the deformation temperatures resulted from heterogeneous, vertical extrusion of the middle to lower crust of the CTMA.

5.2. Kinematic reconstruction

The greatly variable structural patterns of the domains described in Section 3 are an expression of the changing state of strain, yielding a complicated kinematic scenario. Upright cylindrical folds with WNW–ESE striking axial planes and horizontal hinge lines in domains B-2, 4, K-1, and K-4

indicate these domains deformed through NNE–SSW directed compressional stress; the strain state is subhorizontal flattening. Mylonite zones mainly along its southern margin characterize the structures of domain B-3. The mylonitic fabric along the southern margin of domain B-3 is strongly planar with orthorhombic symmetry. Even for the ultramylonite, where stretching lineations are obvious, fabric elements keep an orthorhombic symmetry. Shear sense criteria are rarely seen at field and microscopic scale. Such fabrics indicate a dominantly coaxial subhorizontal stretching for the mylonite under a NNE–SSW directed compressional stress for domain B-3.

In contrast, domains B-1 and K-2 where earlier Devonian plutons are the major deformation media have different structure patterns. The common development of L-type mylonite indicates the strain state of the domains is stretching along the intrusive contact of plutons. Gradual changes in the strike and dip of the foliation, the constant horizontal plunge of the lineation, as well as top-to-the WNW shear direction suggest that the plutons in the domains extrude eastward during deformation via subhorizontal stretching.

It is noteworthy that the boundary between the domains K-3 and K-4 is a NNE-dipping thrust that puts the granulite-facies metamorphic ophiolite suite on the top of the very low graded sedimentary rocks to the south. Taking into account the similar high-temperature deformation of both domains K-2 and K-3, the thrust may represent the footwall of a vertically extruded wedge, although its hanging wall to the north does not display apparent northward normal faulting. The above kinematic discussions are shown as cartoon depictions in Figs. 3g and 4d.

5.3. Interpretation

5.3.1. Structures in the CTMA: vertical and lateral strain partitioning

The fold and thrust structures in the CTMA can be interpreted in a fairly straightforward fashion as a result of NNE–SWS directed compressional tectonic stress. Furthermore, it is reasonable to infer that the tectonic stress resulted from the continent–continent collision between the Tarim Plate and the Illi-central Tianshan micro-continent.

There are many possible causes for the orogen-paralleled stretching lineation. The two most probable situations are: (1) thrust faulting is followed by striking-slip shearing (Vauchez and Nicolas, 1991); (2) strain partitioning during transpressional convergence (Tikoff and Greene, 1997). Other causes include polycyclic deformation overprinting and modification by progressive deformation (Neves et al., 2005). The mylonite zones with subhorizontal stretching lineation in the CTMA appear not to be the result of any of the above outlined causes, because: (1) isotopic and geochronological data indicate the different structural patterns in the CTMA are the result of a monocyclic tectonic evolution and no evidence for structural overprinting was identified. (2) Most structural fabrics have an orthorhombic symmetry, suggesting a bulk NNE–SSW directed, orthogonal compressional tectonic stress field; thus the situation of transpressional convergence can be excluded. However, Chen et al. (1999) emphasized that the southern Tianshan orogeny is an obliquely collisional one based on an integrative study of sedimentology, geochemistry, isotopic geochronology, paleontonology, and paleomagnetism, but unfortunately the study lacked detailed structural observations. (3) The occurrence of shear zones in the CTMA is strongly related to the distribution of isolated earlier Devonian plutons; there is no orogen-scale shear zone. More importantly (4) the change in foliation strike and dip and stable WNW–ESE trending lineation of the domains B-1 and K-2 defines an anticline, and consistent top-to-west shear sense suggests a channel flow kinematic scenario.

Geological mapping reveals that the primary CTMA was a micro-continent with Precambrian crystalline basement, which was intruded by numerous early Devonian calc-alkalic plutons, then covered by Lower Carboniferous sedimentary rocks. A Precambrian crystalline basement is commonly thought having higher competence than Phanerozoic felsic rocks. Thus, the middle to lower crust of the CTMA comprises a heterogeneous aggregate of individual plutons in a crystalline basement matrix, the ''starting material'' for the subsequent deformation. Under coaxial deformation of the heterogeneous media of the CTMA, strain partitioning appears inevitable. The crystalline basement with higher competence forms a load-bearing framework, while the weaker plutons flow with a higher strain ratio. Such a stress situation favors stretching as the strain state for the deformed plutons, which is indicated by common development of L-tectonites. Progressively subhorizontal flow of this weaker material shows a subhorizontal strain partitioning and lateral escape of material during continent–continent collision.

The deformation temperature estimation demonstrated that crustal slices from different levels are juxtaposed in the CTMA. Our $^{40}Ar/^{39}Ar$ geochronological data indicated that the middle to lower crustal mylonite (deformation $T \cong 500–600\ ^{\circ}C$) had been exhumed to middle to upper crustal levels ($T < 335 \pm 50\ ^{\circ}C$) at ca. 300 Ma, suggesting vertical extrusion of middle to lower crust during the convergence although the orogen-perpendicular lineation is not very developed except in the thrust between the domains K-3 and K-4.

Such a configuration of both horizontal and vertical extrusions appears to not be uncommon during coaxial compression, especially for a compressed hot and weak lithosphere (Cagnard et al., 2006). Cagnard et al. (2005, 2006) have experimentally simulated a similar kinematic pattern through a series of analogue experiments on three-layer brittle-ductile models, where the major conclusion is ''horizontal shortening is accompanied by lateral escape'' and ''faults may be accompanied by pop-down and pop-up structures''; obviously, the pop-up structures are equal to vertical extrusion structures of the CTMA.

5.3.2. Structures in the STFT and tectonic implications

Our structural observations indicate the southern Tianshan fold and thrust belt has a doubly-vergent deformation pattern with orthorhombic symmetrical fabrics, at least within its northern part. Such a double vergence is expected to favor a nearly horizontal σ_1 axis (Davis and Engelder, 1985),

although Bonini (2007) suggested much more complicate additional controlling factors leading to the structural styles. The structures of the Tianshan range display (1) a rather distributed crustal shortening marked by regional scale steeply dipping foliations, and (2) juxtaposition of domains from different structural levels. We suggest a thick-skinned structural style for the Tianshan orogen where basements of the CTMA and STFT were involved in deformation. The consistently nearly vertical, WNW–ESE striking axial plane of the folds suggest the nearly horizontal σ_1 is orogen-perpendicular, in contrast with the prediction of the oblique collision model of Chen et al. (1999). Paleomagnetic data (Li, 1990) suggested a rapid northward drift accompanied with an anticlockwise rotation of the Tarim Plate during the Late Devonian to Early Carboniferous, then causing a collision with the Illi-Central Tianshan micro-plate in the late Carboniferous. Meanwhile, the southern Tianshan oceanic crust evolved to be a west-facing remnant oceanic basin. This suggestion is consistent with sedimentological observations (Wang, 1999), and is supported by the $^{40}Ar/^{39}Ar$ data of this study. Paleomagnetic data (Li et al., 1988) also revealed the Tarim Plate clockwise rotated ca. 26° with respect to the Illi-central Tianshan micro-plate during late Carboniferous to earlier Permain, which closed the remnant oceanic basin in a ''scissors-like'' manner. It is reasonable to suggest that the ''scissors-like'' closing and/or the clockwise rotation of the Tarim Plate was caused by a diachronous collision of the two plates that started in the study area around late Carboniferous time. Thus, collision of a rotating block with a stable block does not necessarily result in transpressional deformation along the suture, but, in contrast, it may be that the diachronous collision causes the block rotation.

6. Conclusions

The studied eastern segment of the Illi-central Tianshan micro-continent has experienced a bulk coaxial compressional strain resulting from the orthogonal collision between the Tarim Plate and the Illi-central Tianshan micro-continent in the late Carboniferous. The deformation was progressive during at least a 10 Ma time interval. Partitioning of both strain intensity and kinematics occurred at several scales simultaneously, illustrated by the great variability of structural patterns within the central Tianshan unit. Furthermore, the strain and kinematic partitioning at different scales may have resulted from the deformation of a heterogeneous media, which is comparable and consistent with the results of numerous analogue experimental and numerical modeling.

Acknowledgements

This study is financially supported by the National Basic Research Program of China (973 Program, No. 2007CB411306 and 2001CB409810). We thank Dr Xiao Wenjiao, Domingo Aerden, and J. Hippertt for their thoughtful comments and suggestions. Special thanks are given to Dr Laura Webb for her help with the English text and grammar.

Appendix A. Supplementary data

Supplementary data associated with this article can be found at doi:10.1016/j.jsg.2007.08.002.

References

Allen, B.M., Windley, B.F., Zhang, C., 1992. Paleozoic collisional tectonics and magmatism of the Chinese Tienshan, central Asia. Tectonophysics 220, 89–115.

Bonini, M., 2007. Deformation patterns and structural vergence in brittle-ductile thrust wedges: an additional analogue modeling perspective. Journal of Structural Geology 29, 141–158.

Cagnard, F., Durrieu, N., Gapais, D., Brun, J.-P., Ehlers, C., 2005. Crustal thickening and lateral flow during compression of hot lithospheres, with particular reference to Precambrian times. Terra Nova 18, 72–78.

Cagnard, F., Brun, J.-P., Gapais, D., 2006. Modes of thickening of analogue weak lithospheres. Tectonophysics 421, 145–160.

Carroll, A.R., Graham, S.A., Chang, E.Z., McKnight, C., 2001. Sinian through Permain Tectonostratigraphic evolution of the northwest Tarim basin, China. In: Hendrix, M.S., Davis, G.A. (Eds.), Paleozoic and Mesozoic Tectonic Evolution of Central and Eastern Asia: From Continental Assembly to Intracontinental Deformation. Memoir. Geological Society of America 194, pp. 47–70.

Che, Z.C., Liu, L., Liu, H.F., 1994. Formation and Evolution of the Middle Tianshan Orogenic Belt. Geological Publish House, Beijing.

Chen, C., Lu, H., Jia, D., Cai, D., Wu, S., 1999. Closing history of the southern Tianshan oceanic basin, western China: an oblique collisional orogeny. Tectonophysics 302, 23–40.

Cunningham, D., Owen, L., Snee, L., Li, J.-L., 2003. Structural framework of a major intracontinental orogenic termination zone: the easternmost Tien Shan, China. Journal of the Geological Society London 160, 575–590.

Davis, D.M., Engelder, T., 1985. The role of salt in fold and thrust belt. Tectonophysics 119, 67–88.

Davis, G.H., Reynolds, S.J., 1996. Structural Geology of Rocks and Regions. John Wiley & Sons Inc, New York.

Ernst, W.G., 2005. Alpine and Pacific styles of Phanerozoic mountain building: subduction-zone petrogenesis of continental crust. Terra Nova 17, 165–188.

Gao, J., Li, M., Xiao, X., Tang, Y., He, G., 1998. Paleozoic tectonic evolution of the Tianshan orogen, northwest China. Tectonophysics 287, 213–231.

Goodwin, L.B., Tikoff, B., 2002. Competency contrast, kinematics, and the development of foliations and lineations in the crust. Journal of Structural Geology 24, 1065–1085.

Hames, W.E., Bowring, S.A., 1994. An empirical evaluation of the argon diffusion geometry in muscovite. Earth and Planetary Science Letters 124, 161–169.

Handy, M.R., 1990. The solid-state flow of polymineralic rocks. Journal of Geophysic Research 96, 8647–8661.

Hanmer, S., Passchier, C., 1991. Shear-sense Indicator: a Review. Geological Survey of Canada, Paper. 90–17.

Hao, J., Liu, X., 1993. Ophiolite mélange time and tectonic evolution model of south Tianshan area. Scientia Geologica Sinica 28, 93–95.

Harrison, T.M., Ducan, I., McDougall, I., 1985. Diffusion of ^{40}Ar in biotite: temperature, pressure and compositional effects. Geochimica et Cosmochimica Acta 49, 2461–2468.

Hendrix, M.S., Graham, S.A., Carroll, A.R., Sobel, E.R., McKnight, C.L., Schulein, B.J., Wang, Z.X., 1992. Sedimentary record and climatic implications of recurrent deformation in the Tianshan: evidence from Mesozoic strata of the north Tarim, south Junggar, and Turpan basins, northwest China. Geological Society of America Bulletin 104, 53–79.

Heubeck, C., 2001. Assembly of central Asia during the middle and late Paleozoic. In: Hendrix, M.S., Gregory, A.D. (Eds.), Paleozoic and Mesozoic Tectonic Evolution of Central and Eastern Asia: From Continental Assembly to Intracontinental Deformation. Memoir, vol. 194. Geological Society of America, pp. 1–22.

Jahn, B.M., Griffin, W.L., Windley, B., 2000a. Continental growth in the Phanerozoic: evidence from Central Asia. Tectonophysics 328, viii–x.

Jahn, B.M., Wu, F.Y., Chen, B., 2000b. Massive granitoid generation in Central Asia: Nd isotope evidence and implication for continental growth in the Phanerozoic. Episode 23, 82–97.

Jones, R.R., Holdsworth, R.E., McCaffrey, K.J.W., Clegg, P., Tavarnelli, E., 2005. Scale dependence, strain compatibility and heterogeneity of three dimensional deformation during mountain building: a discussion. Journal of Structural Geology 27, 1190–1204.

Kretz, R., 1983. Symbols for rock-forming minerals. American Mineralogist 68, 277–279.

Lanphere, M.A., Baadsgaard, H., 1997. The Fish Canyon Tuff: a Standard for Geochronology. AGU Abstract with Program 78, p. 326.

Laurent-Charvet, S., Charvet, J., Monie, P., Shu, L., 2003. Late Paleozoic strike-slip shear zones in eastern central Asia (NW China): new structural and geochronological data. Tectonics 22, doi:10.1029/2001TC901047.

Li, Q.G., Liu, S.W., Wang, Z.Q., Han, B.F., Su, G.M., Wang, T., in press. Late Palaeozoic tectonothermal events in the Chinese Tianshan: constraints from electron microprobe monazite ages. Journal of Geological Society London.

Li, Y.J., Sun, L., Wu, H., Wang, G., Yang, C., Peng, G., 2005. Permo-Carboniferous radiolaria from the Wupatarkan Group, west terminal of Chinese South Tianshan. China Journal of Geology 40, 220–226.

Li, Y.P., 1990. An apparent polar wander path from the Tarim block, China. Tectonophysics 181, 31–41.

Li, Y.P., McWilliams, M., Cox, A., Sharps, R., 1988. Upper Permain paleomagnetic poles from dikes of the Tarim craton, China. Geology 16, 275–278.

Lin, S., Williams, P.F., 1992. The origin of ridge-in-groove slickenside striae and associated steps in an S-C mylonite. Journal of Structural Geology 14, 315–321.

Ludwig, K.R., 2003. Isoplot/EX, rev. 3.00, a geochronological toolkit for Microsoft Excel. In: Special Publication, vol. 4. Berkeley Geochronology Center. 71.

McDougall, I., Harrison, T.M., 1999. Geochronology and Thermochronology by the $^{40}Ar/^{39}Ar$ method. Oxford University Press, New York, pp. 1–269.

Neves, S.P., Rangel de Silva, J.M., Mariano, G., 2005. Oblique lineations in orthogneiss and supracrustal rocks: vertical partitioning of strain in a hot crust (eastern Borborema Province, NE Brazil). Journal of Structural Geology 27, 1513–1527.

Passchier, C.W., Trouw, R.A.J., 2005. Micro-tectonics, 2nd ed. (revised and enlarged). Springer-Verlag, Berlin.

Ramsay, J.G., 1967. Folding and Fracturing of Rocks. McGraw-Hill Book Company, New York.

Ramsay, J.G., Lisle, R.J., 2000. Applications of Continuum Mechanics in Structural Geology. In: The Techniques of Modern Structural Geology, vol. 3. Academic Press, London.

Rossetti, F., Faccenna, C., Ranalli, G., 2002. The influence of backstop dip and convergence velocity in the growth of viscous doubly-vergent orogenic wedges: insights from thermomechanical laboratory experiments. Journal of Structural Geology 24, 953–962.

Sengor, A.M.C., Natal'in, A., Burtman, V.S., 1993. Evolution of the Altaid tectonic collage and Paleozoic crustal growth in Eurasia. Nature 364, 299–307.

Spear, F.R., 1993. Metamorphic Phase Equilibria and Pressure Temperature Time Paths. Mineralogic Society of America. Monograph 799.

ten Grotenhuis, S.M., Trouw, R.A.J., Passchier, C.W., 2003. Evolution of mica fish in mylonitic rocks. Tectonophysics 372, 1–21.

Tikoff, B., Greene, D., 1997. Stretching lineations in transpressional shear zone: an example from the Sierra Nevada Batholiths, California. Journal of Structural Geology 19, 29–39.

Upton, P., Koons, P.O., Eberhart-Phillips, D., 2003. Extension and partitioning in an oblique subduction zone, New Zealand: constraints from three-dimensional numerical modeling. Tectonics 22 (doi: 1029/2002TC001431).

Vauchez, A., Nicolas, A., 1991. Mountain building: strike-paralleled motion and mantle anisotropy. Tectonophysics 185, 183–201.

Wang, J.S., 1999. Devonian to Carboniferous Proto-basin reconstruction and tectonic evolution of middle to eastern segment of the Southern Tianshan belt. PhD thesis, Chinese University of Geosciences, Beijing.

Wang, R., Wang, Y., Li, H.M., Zhou, D.W., Wang, J., 1998. Zircon U-Pb ages and its geological significance of high-pressure granulite facies terrane in the Yushugou area, southern Tianshan mountain. Geochimica 27, 517–522.

Windley, B.F., Allen, M.B., Zhang, C., Zhao, Z., Wang, G., 1990. Paleozoic accretion and Cenozoic redeformation of the Chinese Tienshan range, central Asia. Geology 18, 128–131.

Wu, W., Jiang, C., Yang, F., 1990. Petrologic and mathematic Geology studies on the Silurian sedimentary rocks, south of Kumish, Xinjiang. Xinjiang Geological Sciences (series 2), 99–112.

Xiao, W.-J., Zhang, L.-C., Qin, K.-Z., Sun, S., Li, J.-L., 2004. Paleozoic accretionary and collisional tectonics of the Eastern Tianshan (China): implications for the continental growth of central Asia. American Journal of Science 304, 370–395.

Xiao, W.J., Han, C.M., Yuan, C., Chen, H.L., Sun, M., Lin, S.F., Li, Z.L., Mao, Q.G., Zhang, J.E., Sun, S., Li, J.L., 2006. The unique Carboniferous-Permian tectonic-metallogenic framework of Northern Xinjiang (NW China): constraints for the tectonics of the southern Paleoasian Domain. Acta Petrologica Sinica 22, 1362–1376.

Xiao, X., Tang, Y., Feng, Y., Zhu, B., Li, J., Zhao, M., 1992. Tectonic Evolution of Northern Xinjiang and its Adjacent Regions. Geological Publishing House, Beijing.

Xu, X.-W., Ma, T.-L., Sun, L.-Q., Cai, X.-P., 2003. Characteristics and dynamic origin of the large-scale Jiaoluotage ductile compressional zone in the eastern Tianshan Mountains, China. Journal of Structural Geology 25, 1901–1915.

Yang, T.N., Li, J.Y., Sun, G.H., Wang, Y.B., 2006. Earlier Devonian active continental arc in central Tianshan: evidence of geochemical analyses and zircon SHRIMP dating on mylonitized granitic rocks. Acta Petrologica Sinica 22, 41–48.

Yang, T.N., Wang, X.P., 2006. Geochronology, petrochemistry and tectonic implications of earlier Devonian plutons in Kumish area. Xinjiang. Acta Petrologica et Mineralogica 25, 401–411.

Yang, T.N., Li, J.-Y., Sun, G.-H., Wang, Y.B., in press. Meso-proterozoic continental arc type granite in the Central Tianshan mountains (NW China): zircon SHRIMP U-Pb dating and geochemical analyses. Acta Geologica Sinica (English edition; in press).

Zhang, L.F., Ai, Y.L., Li, Q., Li, X.P., Song, S.G., Wei, C.J., 2005. The formation and tectonic evolution of UHP metamorphic belt in southwest Tianshan, Xinjiang. Acta Petrologica Sinica 21, 1029–1038.

Zheng, Y.D., Wang, T., Ma, M., Davis, G.A., 2004. Maximum effective moment criterion and the origin of low-angle normal faults. Journal of Structural Geology 26, 271–285.

Zhou, D., Graham, S.A., Chang, E.Z., Wang, B., Hacker, B., 2001. Paleozoic tectonic amalgamation of the Chinese Tianshan: evidence from a transect along the Dushanzi-Kuqa highway. In: Hendrix, M.S., Gregory, A.D. (Eds.), Paleozoic and Mesozoic Tectonic Evolution of Central and Eastern Asia: From Continental Assembly to Intracontinental Deformation. Memoir, vol. 194. Geological Society of America, pp. 23–46.

Zhou, D.W., Su, L., Jian, P., Wang, R., Liu, X., Lu, G., Wang, J., 2004. Zircon SHRIMP U-Pb dating on the high-pressure granulite facies terrane of the Yushugou ophiolite suit, and its tectonic implications, south Tianshan. Chinese Science Bulletin 49, 1411–1415.

Zhu, Y.F., Zhang, L.F., Gu, L.B., Guo, X., Zhou, J., 2005. Zircon SHRIMP geochronology and trace elements of Carboniferous volcanic rocks from eastern Tianshan. Chinese Science Bulletin 50, 2004–2014.